Comparison of Methods to Examine Sub-Synchronous Oscillations Caused by Grid-Connected Wind Turbine Generators

Wenjuan Du, *Member, IEEE*, Bixing Ren, Haifeng Wang, *Senior Member, IEEE*, and Yang Wang

***Abstract*—This paper compares three methods, the impedance model based analysis, the positive net damping analysis, and the open-loop modal resonance analysis. The differences and connections among these three methods are revealed, which helps to gain better understanding on the limitations of the methods for studying the mechanism of sub-synchronous oscillations (SSOs) caused by grid-connected wind turbine generators (WTGs) in a power system. Following useful conclusions are obtained, which are evaluated and demonstrated by study cases: First, both the negative resistance and negative net damping are highly related with strong dynamic interactions between the WTGs and ac grid under the condition of modal resonance. This explains why resistance and net damping may become negative from the standpoint of system modal condition. Second, it is possible that results of impendence model based analysis (IMA) and positive net damping analysis (PDA) may not reflect correctly the system SSO instability risk brought about by the WTGs. The reason is that the IMA and PDA are based on the sufficient condition of system stability. Assessment made by the IMA or PDA may be very conservative. In study cases, three methods are compared in the parameter space of converter controllers of the WTGs such that all the parameter conditions are covered in comparison.**

***Index Terms*—Sub-synchronous oscillations (SSO), grid-connected wind turbine generators, impedance model based analysis, positive net damping analysis, open-loop modal resonance analysis.**

I. Introduction

GRID-CONNECTED wind turbine generators (WTGs) may bring about risk of oscillations in a power system. For example, it has been found that with the increase of penetration level of wind or lack of reactive power support, damping of power system electromechanical power oscillations may degrade [1]–[4]. Further detailed investigation reveals that the WTGs may have low-frequency oscillation modes which are the sources of instability risk [2], [5], [6]. Improper parameters setting of the phase locked loop (PLL) and converter controllers as well as condition of weak grid connection are key factors for a grid-connected WTG to cause sub-synchronous oscillations (SSOs) [7], [8]. Study presented in [1]–[8] has focused on examining the physical causes of the WTGs to induce power system oscillations, identifying the physical components which are responsible for the oscillations. The study has helped considerably to gain better understanding about the oscillation mechanism from the engineering perspective, such as the penetration level [1], [2], function of reactive power support [3], [4], existence of low-frequency oscillation modes of WTGs [5], [6], role of parameters setting of PLL and converter controllers as well as the condition of grid connection of WTGs [7], [8].

In order to examine the general mechanism of the SSOs induced by grid-connected WTGs, rather than to identify the physical components of concern, three main methods have been proposed and used so far. They are the impendence model based analysis (IMA), positive net damping analysis (PDA) and open-loop modal resonance analysis (OMA). The IMA has been the most widely recognized and accepted method to examine the SSO mechanism generally. The examination divides the power system into the WTG subsystem and the subsystem of remainder of the power system (ROPS subsystem). The IMA assesses the stability of interconnected system comprised of two subsystems according to the Nyquist stability criterion. It attributes the cause and risk of SSOs to the negative resistance contributed by the WTG [9]–[13].

More recently appeared PDA is also based on the Nyquist stability criterion. It was proposed in [14] and proved being effective in examining the SSOs caused by grid-connected WTGs [15]. Applications of the IMA and PDA require only the open-loop frequency-domain information of the WTG and ROPS subsystems. The open-loop information may be obtained from measurement data at the interface between the grid-connected WTG and the ROPS. This is the main advantage of the IMA and PDA. The PDA is an alternative method to the IMA, attributing the cause of SSO danger to the negative net damping. However, the difference and connection between the IMA and PDA has not been studied so far.

Manuscript received November 21, 2018; revised March 27, 2019; accepted April 20, 2019. Date of publication June 3, 2019; date of current version October 24, 2019. This work was supported by the State Grid Corporation of China under Grant NYB17201800102. Paper no. TPWRS-01767-2018. *(Corresponding author: Haifeng Wang.)*

W. Du is with the School of Electrical Engineering, Sichuan University, Chengdu 610017, China (e-mail: ddwenjuan@qq.com).

B. Ren is with the State Grid Jiangsu Electric Power Company Ltd. Research Institute, Nanjing 211101, China (e-mail: renbixing@126.com).

H. Wang and Y. Wang are with the State Key Laboratory of Alternate Electric Power Systems With New Energy Resources, North China Electric Power University, Beijing 102206, China (e-mail: hfwang60@qq.com; wangyang_ncepu@126.com).

Color versions of one or more of the figures in this paper are available online at http://ieeexplore.ieee.org.

Digital Object Identifier 10.1109/TPWRS.2019.2920416

The OMA was proposed particularly to reveal the general mechanism of the SSOs caused by the grid-connected WTGs from the perspective of modal conditions [16]. From the modal information of open-loop WTG and ROPS subsystems, the OMA can detect the SSO risk of interconnected power system with the WTG. The OMA attributes the SSO risk to the proximity of SSO modes of WTG and ROPS subsystems, which is referred to as the open-loop modal resonance [16]. It is of the potential to extend the main advantage of IMA and PDA in applying the modal analysis by using the measurement data.

The IMA, PDA and OMA are proposed for the same purpose to study the general mechanism of the SSOs caused by grid-connected WTGs. They provide different explanations from the standpoints of negative resistance, negative net damping and modal resonance respectively about why the grid-connected WTGs may cause the SSOs. For a same case of the SSOs caused by the WTGs, different results may be obtained when three methods are applied separately. Why and how may the results be different? Which result could be closer to the truth and why? Are there any connections among the results and why? Finding the answers to those important questions has motivated the work presented in this paper.

The paper compares the differences and connections between the IMA, the PDA and the OMA. The comparison helps to gain a better understanding on the limitations of those three methods in application. Analytical comparison indicates that: (1) Although criteria of the IMA and PDA to assess system stability look same, results of assessment may be different, because the value of frequency to apply the criteria is different; (2) The IMA and PDA are related with the OMA. The relation explains why resistance and net damping may become negative from the standpoint of system modal condition. When the modal resonance happens, resistance and net damping degrades. However, results of the IMA and PDA may be more conservative than that of the OMA; (3) The IMA and PDA may not be able correctly to indicate the degree of system stability degradation caused by the grid-connected WTGs, because they are based on the sufficient condition of stability of single-input single-output closed-loop system. Indication made by the IMA and PDA may be meaningless or even wrong. Hence, in application, extra care needs to be taken to interpret the results obtained by the IMA and PDA.

Study cases for two example power systems with grid-connected WTGs are presented to evaluate and demonstrate the analysis and conclusions made in the paper. It was found that the improper parameters setting of the PLL and the current control inner loop (CCIL) are the physical causes for the grid-connected WTGs to induce power system oscillations [2]–[6] and the SSOs [7], [8], [11], [13]. Hence, in the first example, the impact of parameters setting of the PLL of a grid-connected PMSG on the SSOs is examined. In the second example, the effect of the CCIL of rotor side converter (RSC) of a grid-connected DFIG is studied. Considering the fact that numerical results of comparison may be sensitive to the setting values of parameters of the PLL and the CCIL, the SSO stability regions of example power systems, rather than the single-point SSO stability, in the parameter space of the PLL or the CCIL are used for the evaluation of system stability in order to cover fully all the possible cases. Study cases of comparison clearly demonstrate the following aspects of power system SSOs which may not be found when only one of three methods is applied. (1) Stable regions worked out by the IMA and PDA reduce accordingly with the decrease of true stable regions of the example power system with the WTGs. The reduction is caused by the dynamic interactions between the WTGs and AC grid, which are strongest under the condition of modal resonance. Hence, dynamic interactions cause the decrease of resistance and net damping of the WTGs, which may become negative when the modal resonance happens. (2) The results of IMA and PDA are much more conservative than that of OMA in detecting the system instability risk caused by the WTGs. Degree of system instability risk may be wrongly indicated by the results of IMA and PDA. The paper is organized as follows.

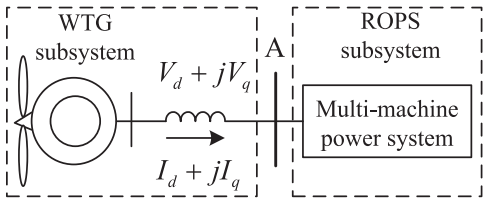

Fig. 1. A power system integrated with a grid-connected WTG.

In the next section, firstly the methods of IMA and PDA are briefly reviewed. Their merits and disadvantages are generally discussed. Key issues about the methods, which need to be further examined and addressed, are raised. Possible reasons that they may generate incorrect results of stability assessment are explained in the parameter space of system stability. Secondly, the method of OMA is briefly reviewed. Main advantages and drawbacks of OMA are discussed. Directions of potential further investigation and improvement are pointed out. Connections between the IMA and OMA are derived. The derivation indicates their difference when they are applied to detecting the SSO risk caused by the grid-connected WTG.

Study cases are presented in Sections III and IV. Final section of the paper summarizes the main conclusions obtained and novel contributions made by the paper.

II. Method of IMA, PDA and OMA

A. Method of IMA

Fig. 1 shows the configuration of a power system with a grid-connected WTG. At point A (usually the PCC of WTG), the power system can be divided into WTG and ROPS subsystem. For example, denote $I_d + jI_q$ and $V_d + jV_q$ as the current output from and terminal voltage of the WTG at point A respectively, both of which are expressed in the $d-q$ coordinate of the WTG. An interconnected model is established and depicted by Fig. 2. In Fig. 2, $\mathbf{H}(s)$ and $\mathbf{G}(s)$ are separately the transfer function matrix of WTG and ROPS subsystem.

If the interactions between d and q components of variables in Fig. 2 are ignored, non-diagonal elements of $\mathbf{H}(s)$ and $\mathbf{G}(s)$ are zero. Under this assumption (denoted as *assumption 1* for the convenience of discussions), the two-input two-output (TITO)

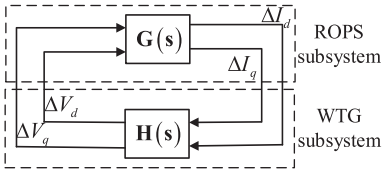

Fig. 2. Interconnected model of power system with a WTG.

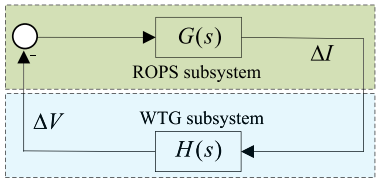

Fig. 3. Simplified SISO interconnected model under *assumption 1*.

interconnected model of Fig. 2 is simplified to a single-input single-output (SISO) interconnected model shown by Fig. 3 [11]. Alternatively, by using the positive and negative sequence expression of current and voltage, a TITO interconnected model similar to that shown by Fig. 2 can also be derived. To simplify the TITO interconnected model to the SISO interconnected model shown by Fig. 3, it is assumed that there are no interactions between positive and negative sequential variables [17]. This is the alternative form of *assumption 1*. In Fig. 3, ΔI and ΔV are the d and q or positive and negative sequential components of current and voltage displayed in Fig. 2. $G(s)$ and $H(s)$ are respectively the transfer functions of ROPS and WTG subsystem corresponding to ΔI and ΔV.

In the frequency domain, transfer function of WTG subsystem is effectively an impedance, $Z_h(j\omega) = H(j\omega)$. Impedance of ROPS subsystem is $Z_g(j\omega) = \frac{1}{G(j\omega)}$. The SSO stability of interconnected model shown by Fig. 3 can be assessed by applying the Nyquist or Bode stability criteria to $\frac{Z_h(j\omega)}{Z_g(j\omega)}$. This is why the method is referred to as the IMA. In this paper, the IMA by applying the Nyquist or Bode stability criteria is referred to as the *Nyquist IMA* for the convenience of discussions. There are several simplified formats of IMA to apply the Nyquist or Bode stability criteria, among which the *positive resistance IMA* method is the mostly recognized one [13]. In this paper, the *positive resistance IMA* is referred simply as the IMA method and reviewed briefly as follows.

Denote

$$Z_h(j\omega) = R_h(\omega) + j\omega X_h(\omega), Z_g(j\omega) = R_g(\omega) + j\omega X_g(\omega) \tag{1}$$

Thus,

$$\frac{Z_h(\omega)}{Z_g(\omega)} = \frac{R_h(\omega)R_g(\omega) + \omega^2 X_h(\omega)X_g(\omega)}{R_g(\omega)^2 + \omega^2 X_g(\omega)^2} + j\omega\frac{X_h(\omega)R_g(\omega) - R_h(\omega)X_g(\omega)}{R_g(\omega)^2 + \omega^2 X_g(\omega)^2} \tag{2}$$

At an SSO frequency ω_s, the interconnected system shown by Fig. 3 is stable if following two conditions are met

$$X_h(\omega_s) + X_g(\omega_s) = 0 \tag{3}$$

$$\text{Real part}\left[\frac{Z_h(\omega_s)}{Z_g(\omega_s)}\right] > -1 \tag{4}$$

Hence, the sufficient condition of system stability is obtained from (2), (3) and (4) to be

$$R_g(\omega_s)[R_h(\omega_s) + R_g(\omega_s)] > 0 \tag{5}$$

Normally, the ROPS subsystem is of positive resistance such that $R_g(\omega_s) > 0$. Hence, the sufficient stable condition of interconnected system of Fig. 3 is that the WTG subsystem is of positive resistance at the SSO frequency, ω_s, i.e.,

$$R_h(\omega_s) > 0 \tag{6}$$

The PDA was proposed in [14] to find ω_s by setting the imaginary part of $\frac{Z_h(j\omega)}{Z_g(j\omega)}$ in (2) to zero, from that it can have

$$\frac{X_h(\omega_s)}{X_g(\omega_s)} = \frac{R_h(\omega_s)}{R_g(\omega_s)} \tag{7}$$

Subsequently, from (2), (7) and by setting the real part of $\frac{Z_h(j\omega)}{Z_g(j\omega)}$ to be greater than -1, it can have

$$\frac{R_h(\omega_s)R_g(\omega_s) + {\omega_s}^2 X_h(\omega_s)X_g(\omega_s)}{R_g(\omega_s)^2 + {\omega_s}^2 X_g(\omega_s)^2} > -1 \tag{8}$$

From (7) and (8), the sufficient stable condition of interconnected system is obtained to be

$$\frac{R_h(\omega_s) + R_g(\omega_s)}{R_g(\omega_s)} > 0 \text{ or simply } R_h(\omega_s) > 0 \tag{9}$$

In [14], $R_h(\omega_s) + R_g(\omega_s)$ or $R_h(\omega_s)$ is referred to as the net damping. From (5) and (9), it can be seen that net damping and resistance are same.

Following remarks can be made by comparing the method of IMA and PDA reviewed above.

1) As it has been pointed out in Section I, most important advantage of IMA and PDA is in practical applications. For example, it can guide the grid connection of or/and the design of supplementary damping controller for the WTG to evade the negative impact of the WTG on power system SSO stability without having to derive system parametric model. However, both the IMA and PDA are sufficient stability criterion. They cannot be used directly to detect the SSO instability risk brought about by the WTG, which is important in order to identify the trouble-making WTGs in a complex power system.

This aspect can be demonstrated clearly by a designed study case as follows.

Denote $\hat{\lambda} = -\hat{\xi} + j\hat{\omega}$ as the most poorly damped SSO mode of a power system with a grid-connected WTG. Consider the case that when a parameter of WTG, α, varies, $\hat{\lambda}(\alpha)$ moves along a vertical line in the complex plane, i.e., $\hat{\xi}(\alpha) = c$ where c is a constant. For example, when $c = 0$, the vertical line is the imaginary axis of complex plane. In this case, when α varies, system

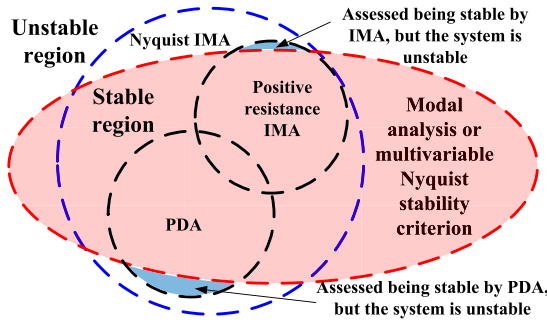

Fig. 4. Stable regions in a parameter space of the WTG.

stability dominated by the SSO mode remains unchanged. However, it is easy to find that when α changes, the resistance of the WTG varies accordingly. This study case indicates that in fact, variation of resistance of the WTG may mean nothing for assessing the system instability risk as caused by the grid-connected WTG, because when the system stability remains same, the result of assessment should be unchanged. In Section III-C, such a study case is presented. Hence, in this aspect, necessary condition of SSO stability needs to be developed from the Nyquist IMA. This has been a vital gap of study yet to be filled in for applying the IMA to examine the mechanism of the SSOs caused by the grid-connected WTG.

2) Criteria of system stability derived in (5) and (9) are same, i.e., positive resistance or net damping. Hence, main difference between the IMA and PDA is (3) and (7) to find the SSO frequency ω_s. Equation (3) is of clear meaning, because ω_s is obviously the resonant SSO frequency between the WTG and ROPS subsystems. However, if equations (3) and (7) are met simultaneously, it can have

$$\frac{X_h(\omega_s)}{X_g(\omega_s)} = \frac{R_h(\omega_s)}{R_g(\omega_s)} = -1 \tag{10}$$

Thus, equations (5) and (9) become inapplicable. This implies that results of the IMA and PDA are different and complementary to each other. If they are applied jointly, a less conservative assessment about the SSO stability may be obtained. However, it has been unknown how conservative both the IMA and PDA are.

In a parameter space of a grid-connected WTG, stable region of the power system with the grid-connected WTG can be obtained by applying either the modal analysis or the multivariable Nyquist stability criterion [17] based on the TITO interconnected model of Fig. 2. This is true stable region as shown by the shadowed area in Fig. 4. Stable region obtained from the SISO interconnected model of Fig. 3 is the area surrounded by the solid curve. Its difference with the shadowed area is caused by *assumption 1*. Stable regions obtained by the positive resistance IMA (i.e., IMA) or PDA are inside the areas surrounded by the dashed curves. It can be seen that if *assumption 1* does not stand, assessment from the IMA or PDA may even not sufficient to ensure the SSO stability of the power system with the WTG, because in the areas highlighted in dark in Fig. 4, the system was assessed by the IMA and PDA being stable but in fact it is unstable. In Section IV-B, such a study case is presented.

Another essentially important issue is the relative size of various stable regions surrounded by curves in Fig. 4 to that of shadowed area which is the true stable region. Under the condition that *assumption 1* stands, stable regions obtained from TITO and SISO interconnected model are overlapped. However, if the stable regions worked out by the IMA or PDA are too small as compared with the true stable region, either the SSO instability risk may become overstated or operation and grid connection of the WTG may be over restricted. So far, it has been unknown how far away the boundaries of the stable regions worked out by the IMA or PDA are from those of true stable region.

B. Method of OMA

Let the state-space representations of interconnected model and subsystems shown in Fig. 1 be

$$\text{Interconnected model}: \frac{d}{dt}\mathbf{\Delta X} = \mathbf{A}\mathbf{\Delta X} \tag{11}$$

$$\text{WTG subsystem}: \frac{d}{dt}\mathbf{\Delta X_H} = \mathbf{A_H}\mathbf{\Delta X_H} + \mathbf{B_H}\mathbf{\Delta V}$$
$$\mathbf{\Delta I} = \mathbf{C_H}\mathbf{\Delta X_H} + \mathbf{D_H}\mathbf{\Delta V} \tag{12}$$

$$\text{ROPS subsystem}: \frac{d}{dt}\mathbf{\Delta X_G} = \mathbf{A_G}\mathbf{\Delta X_G} + \mathbf{B_G}\mathbf{\Delta I}$$
$$\mathbf{\Delta V} = \mathbf{C_G}\mathbf{\Delta X_G} + \mathbf{D_G}\mathbf{\Delta I} \tag{13}$$

The procedure to apply the OMA is as follows.

1) Calculate all the SSO modes of subsystems from $\mathbf{A_H}$ and $\mathbf{A_G}$ to identify the proximity of any two SSO modes separately from two subsystems (i.e., open-loop modal coupling [16]) on the complex plane. For example, an SSO mode of WTG subsystem, λ_H, is identified to be in the proximity to an SSO mode of ROPS subsystem, λ_G, i.e., $\lambda_H \approx \lambda_G$, which is referred to as the open-loop modal resonance.
2) Calculate following 2×2 residue matrices for λ_H and λ_G respectively.

$$\mathbf{R_H} = \mathbf{C_H}\mathbf{v_H} \times \mathbf{w_H^T}\mathbf{B_H}, \mathbf{R_G} = \mathbf{C_G}\mathbf{v_G} \times \mathbf{w_G^T}\mathbf{B_G} \tag{14}$$

where $\mathbf{w_H}$ and $\mathbf{v_H}$ are the left and right eigenvector of $\mathbf{A_H}$ for λ_H, $\mathbf{w_G}$ and $\mathbf{v_G}$ are the left and right eigenvector of $\mathbf{A_G}$ for λ_G.

3) Denote $\hat{\lambda}_H$ and $\hat{\lambda}_G$ as the SSO modes of interconnected model corresponding to λ_H and λ_G. They can be estimated as

$$\hat{\lambda}_G \approx \lambda_G \pm \sqrt{-\sum diag[\mathbf{R_H}\mathbf{R_G}]}$$
$$\hat{\lambda}_H \approx \lambda_H \pm \sqrt{-\sum diag[\mathbf{R_H}\mathbf{R_G}]} \tag{15}$$

where $diag[\,]$ refers to the diagonal elements of a matrix.

Thus, the SSO instability criterion (SIC) is established from (15) to be

$$\text{SIC} = \left|\text{Real part of } \sqrt{-\sum diag[\mathbf{R_H R_G}]}\right| - |\text{Real part of } \lambda_H \approx \lambda_G| \tag{16}$$

If SIC ≥ 0, the power system with the WTG is unstable. If SIC < 0, the system is stable.

Merits of the OMA outlined above are as follows.

1) The analysis is applicable without having to have *assumption 1*.
2) The SIC is an approximately necessary and sufficient condition of system SSO stability and hence can be used to detect the SSO instability risk.
3) Application of OMA only needs the modal information of subsystems, rather than derivation of interconnected model. This makes it more acceptable in practice when exchange of detailed information between the WTG and power system may be impossible.

Main drawbacks in applying the OMA are as follows.

1) Condition of applying the OMA to assess the system SSO stability is the open-loop modal resonance of subsystems, i.e., $\lambda_H \approx \lambda_G$. It cannot be applied for the cases when the modal resonance may not happen, such as the case that the induction generator effect (IGE) causes the SSOs.
2) Equation (15) is the first-order approximation of SSO modes of interconnected model. Hence, it has been unknown when the SIC defined in (16) may produce incorrect assessment.
3) Further study is urgently needed to apply the OMA based on measurement data, rather than the parametric models of subsystems. In this aspect, modal identification technique may come to help so as to enhance the applicability of the OMA in practice.

C. Connection Between the Method of IMA and OMA

Express the SSO modes in the OMA as

$$\lambda_G = -\xi_G + j\omega_G, \hat{\lambda}_G = -\hat{\xi}_G + j\hat{\omega}_G \tag{17}$$

For the SISO interconnected system of Fig. 3, it can have

$$R_G = (s-\lambda_G)G(s)|_{s=\lambda_G}, R_H = (s-\lambda_H)H(s)|_{s=\lambda_H} \tag{18}$$

Let $R_G R_H = r_{re} + jr_{im}$. From (18),

$$\begin{aligned} G(j\hat{\omega}_M)H(j\hat{\omega}_M) &\approx \frac{R_G R_H}{(j\hat{\omega}_G - \lambda_G)^2} \\ &= \frac{r_{re}[\xi_G^2 - (\hat{\omega}_G - \omega_G)^2] + 2\xi_G(\hat{\omega}_G - \omega_G)r_{im}}{[\xi_G^2 - (\hat{\omega}_G - \omega_G)^2]^2 + [2\xi_G(\hat{\omega}_G - \omega_G)]^2} \\ &\quad + j\frac{r_{im}[\xi_G^2 - (\hat{\omega}_G - \omega_G)^2] - 2\xi_G(\hat{\omega}_G - \omega_G)r_{re}}{[\xi_G^2 - (\hat{\omega}_G - \omega_G)^2]^2 + [2\xi_G(\hat{\omega}_G - \omega_G)]^2} \end{aligned} \tag{19}$$

The frequency of SSOs is $\hat{\omega}_G$. According to the IMA and PDA, if real part of $G(j\hat{\omega}_G)H(j\hat{\omega}_G)$ is greater than -1, the interconnected system of Fig. 3 is stable. For $\hat{\lambda}_G = -\hat{\xi}_G + j\hat{\omega}_G$ and in the neighborhood of $\lambda_G = -\xi_G + j\omega_G$, it can have $\omega_G \approx \hat{\omega}_G$. Thus, from (19) and $\omega_G \approx \hat{\omega}_G$,

$$\text{Real part } [G(j\hat{\omega}_G)H(j\hat{\omega}_G)] \approx \frac{r_{re}}{{\xi_G}^2} > -1 \tag{20}$$

Hence, if $\xi_G^2 > -r_{re}$, the IMA and PDA conclude that the interconnected system of Fig. 3 is stable. From the stability criterion of OMA expressed by (15), it can be seen that if $\xi_G^2 > -r_{re}$, the SIC defined by (16) is negative such that the SISO interconnected system of Fig. 3 is stable.

Derivation above indicates that if the power system with the WTG is assessed by the IMA or PDA to be stable and when the modal proximity happens, the criterion of OMA ensures that the system is stable. This implies that stability assessment by the OMA is not more conservative than that by the IMA and PDA.

Connection between the IMA, the PDA and the OMA derived above indicates that dynamic interactions between the AC grid and the WTG may be highly related with the computational results of the IMA and PDA. Under the condition of modal resonance when the dynamic interactions are strong, negative resistance or negative net damping may occur. This explains generally when the resistance or negative net damping may become negative from the aspect of dynamic interactions, i.e., condition of modal resonance. In the next section, the connection is evaluated and demonstrated by study cases.

III. An Example Power System With Grid-Connected PMSGs

A. Stable Regions in the Parameter Space of the PLL

Fig. 5 shows the configuration of an example power system with wind-thermal bundled generation at the sending end. Model and parameters of synchronous generator (SG) recommended in [18] for studying the sub-synchronous resonance (SSR) are used. Model and parameters of PMSG used in [16] are adopted. Other parameters of the example system are given in Appendix. The PMSG is equipped with the SRF PLL [19]. In this example, the examination is focused on the physical component of the grid-connected PMSG, the PLL [8], [19]. The impact of the PLL on the SSO stability of the example power system is studied to evaluate and demonstrate various aspects of comparison

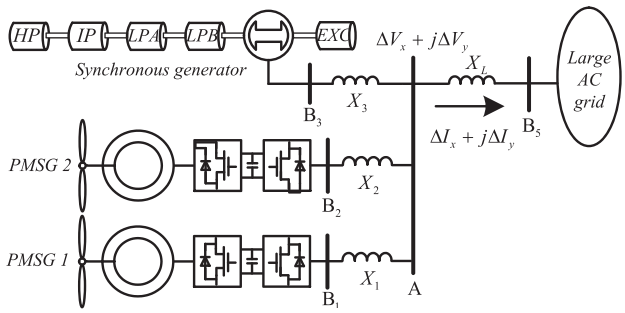

Fig. 5. A power system with wind-thermal bundled generation.

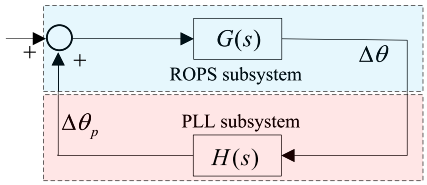

Fig. 6. Interconnected model to examine the impact of PLL1.

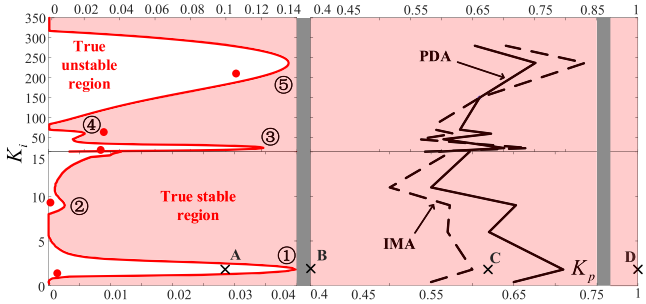

Fig. 7. Stable regions in the parameter space of PLL1.

between the IMA, the PDA and the OMA made in the previous section.

Key parameters of the SRF PLL are the PI gains of closed-loop control, K_p and K_i, for tracking the phase of terminal voltage of a grid-connected PMSG [8], [19]. Thus, stability regions of the first example power system are computed in the two-dimensional parameter space of PLL to compare the methods of IMA, PDA and OMA in detecting the instability risk brought about by the PLL of PMSG1 (referred as PLL1) as follows.

An interconnected model is derived for the first example power system and displayed by Fig. 6, where $H(s)$ is the transfer function of PLL subsystem comprised of PLL1 and $G(s)$ is the transfer function of ROPS subsystem consisted of PMSG2, SG, network and PMSG1 excluding the PLL1 [19]. In Fig. 6, θ is the phase of terminal voltage of PMSG1; θ_p is the tracked phase of θ by PLL1. Transfer function of PLL1 is [19]

$$H(s) = \frac{V_0 K_p s + V_0 K_i}{s^2 + V_0 K_p s + V_0 K_i} \tag{21}$$

where, V_0 is the magnitude of terminal voltage of PMSG1 at steady state and normally $V_0 \approx 1$ p.u.

Computational results of stable regions in the parameter space of PLL1 over the range of SSO frequency are displayed in Fig. 7. Boundary of stable region shadowed in grey is computed from the state matrix of interconnected model shown by Fig. 6 by using the standard method of modal analysis [1]. Hence, it is the true division between the stable and unstable region of the first example power system. Boundaries in black are computed by using the IMA and PDA on the basis of interconnected model of Fig. 6. Following aspects can be observed from the results of comparison displayed in Fig. 7.

1) The boundaries of stable regions computed by IMA and PDA are different. This confirm the analysis made in the previous section about the consequence of difference between (3) and (7) to find the frequency, at which the resistance or net damping is calculated by the IMA or PDA separately.
2) Stable regions computed by IMA and PDA are inside the true stable regions, confirming the analysis about Fig. 4. In addition, the boundaries of stable regions computed by IMA and PDA are quite away from the boundary of true stable region. This confirmed that results of the IMA and PDA to indicate the SSO risk are very conservative. When the IMA and PDA indicate that the system is unstable (negative resistance or negative net damping), it may be quite possible that the system was in fact stable. From the figures displayed in the horizontal axis of Fig. 7 it can be seen that if the proportional gain of the PLL1, K_p, is set as guided by either the IMA or the PDA, it would be set over large by more than 10 times.
3) The trend of variation of boundaries of stable regions computed by IMA and PDA is similar to that of true stable region. With the reduction of true stable regions around point ①, ②, ③, ④ and ⑤ in Fig. 7, stable regions computed by IMA and PDA decrease accordingly.

The aspects outlined above are further investigated in the following subsections.

B. Causes of Reduction of Stable Regions

From (21), it can be seen that stable region of PLL subsystem is the right half of two-dimensional parameter space of PLL1, i.e., $K_p > 0$. Hence, it can be concluded that reduction of true stable region of the example power system as shown in Fig. 7 is caused by the interconnection of PLL subsystem and ROPS subsystem. The interconnection results in dynamic interactions between the PLL and POPS subsystems, leading to the decrease of SSO stability of the example power system. To validate the conclusion, following tests are carried out.

First, according to the theory of OMA, when the open-loop modal resonance happens, strong dynamic interactions between the PLL and ROPS subsystem shall degrade the SSO stability of the power system [19]. Hence, in the range of SSO frequency, the SSO modes of ROPS subsystem are identified by modal computation from open-loop state matrix of ROPS subsystem. They are $\lambda_{ri}, i = 1, 2, 3, 4, 5$ listed in the 1st column of Table I. In addition, physical components associated with the identified SSO modes are found by calculating the participation factors and listed in the 2nd column of Table I.

Second, denote λ_p as the oscillation mode of PLL subsystem in Fig. 6. Open-loop modal resonance between the PLL and ROPS subsystem in Fig. 6 is $\lambda_p \approx \lambda_{ri}, i = 1, 2, 3, 4, 5$. Hence, from the SSO modes of ROPS subsystem listed in the first column of Table I, $\lambda_{ri}, i = 1, 2, 3, 4, 5$ and using $\lambda_p = \lambda_{ri}, i = 1, 2, 3, 4, 5$, values of PI gains of PLL1, K_p and K_i, to cause the modal resonance are computed. Computational results are presented in the third column of Table I as K_{pi} and $K_{ii}, i = 1, 2, 3, 4, 5$. In the two-dimensional parameter space of PLL1, $(K_{pi}, K_{ii}), i = 1, 2, 3, 4, 5$ are five points, which are indicated by black solid circles in Fig. 7. Those are the points where

TABLE I
SSO MODES OF ROPS SUBSYSTEM AND PARAMETERS OF PLL1 TO CAUSE THE OPEN-LOOP MODAL RESONANCE

SSO modes of the ROPS subsystem	Dynamic components associated with the SSO modes	Values of PI gains of PLL1 to cause the modal proximity
$\lambda_{r1} = -1.71 + j22.9$	Reactive power control outer loop of PMSG1	$K_{p1} = 0.0012, K_{i1} = 1.6$
$\lambda_{r2} = -0.07 + j55.4$	The 1st torsional SSO mode of SG	$K_{p2} = 0.0005, K_{i2} = 9.2$
$\lambda_{r3} = -4.88 + j82.3$	Active power Control outer loop of PMSG1	$K_{p3} = 0.0298, K_{i3} = 22$
$\lambda_{r4} = -5.7 + j136$	PLL of PMSG2	$K_{p4} = 0.035, K_{i4} = 56$
$\lambda_{r5} = -15 + j249$	Current control inner loops of GSC of PMSG1	$K_{p5} = 0.104, K_{i5} = 210$

the open-loop modal resonance happened between the PLL subsystem and ROPS subsystem. From Fig. 7, it can be seen that reduction of stable regions occurs around those five points of modal resonance. This indicates the reduction of stable regions is related with the modal resonance.

Third, dynamics of various components identified in the second column of Table I except the control outer loop of PMSG1 are removed from the ROPS subsystem consecutively in three steps. Removal of dynamics eliminates the associated oscillation modes, $\lambda_{ri}, i = 1, 2, 4, 5$ successively. Consequently, the modal resonance, $\lambda_p \approx \lambda_{ri}, i = 1, 2, 4, 5$, disappears one by one in the example power system. Computational results of stable regions with the consecutive removal of dynamics of identified components in three steps are presented in Fig. 8.

At the first step, torsional dynamics of the SG and dynamics of PLL of PMSG2 in the example power system are removed. Thus, the open-loop SSO modes of the ROPS subsystem, $\lambda_{ri}, i = 2, 4$, are eliminated. Computational results of stable regions are displayed in Fig. 8(a). It can be seen that reduction of stable regions around point ② and ④ in Fig. 7 disappears accordingly with the dismissal of modal resonance, $\lambda_p \approx \lambda_{ri}, i = 2, 4$.

At the second step, dynamics of current inner control loops of GSC of PMSG1 are excluded from the ROPS subsystem such that λ_{r5} is eliminated. Stable regions are shown by Fig. 8(b). It can be seen that the reduction of stable regions around point ⑤ disappears with the elimination of model resonance, $\lambda_p \approx \lambda_{r5}$.

At the third step, reactive power control outer loop of GSC of PMSG1 is excluded from the ROPS subsystem. Computational results of stable regions are presented in Fig. 8(c). It can be seen that the reduction of stable regions around point ① also disappears. In order to clearly show the results of elimination of modal resonance, in Fig. 8(c), boundaries of stable regions displayed in Fig. 7 before the removal of $\lambda_{ri}, i = 1, 2, 4, 5$ are redrawn in dashed curves. Note that with the successive removal of dynamics of components associated with the SSO modes of open-loop ROPS subsystem, computational results by using the PDA are very similar to those of the IMA displayed in Fig. 8.

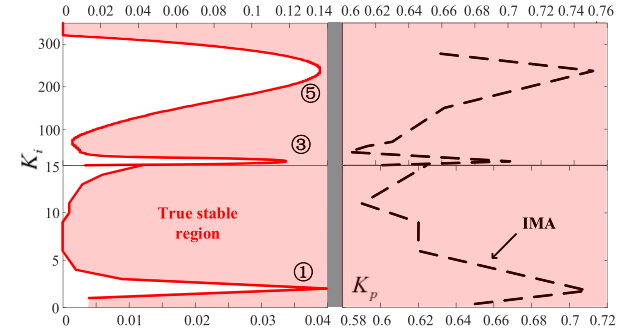

(a) Torsional dynamics of SG and dynamics of PLL of PMSG2 are removed such that reduction of stable region around ② and ④ disappears

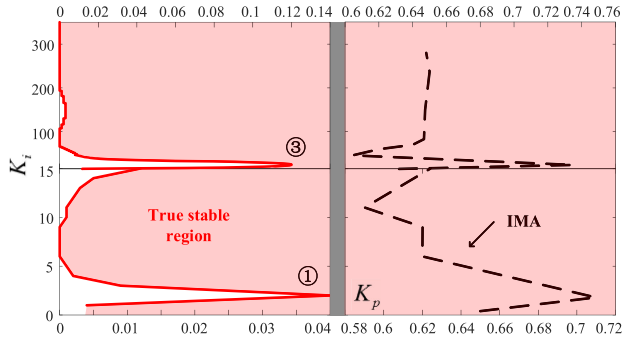

(b) Torsional dynamics of SG, dynamics of PLL of PMSG2 and current control inner loops of PMSG1 are removed such that reduction of stable region around ② , ④ and ⑤ disappears

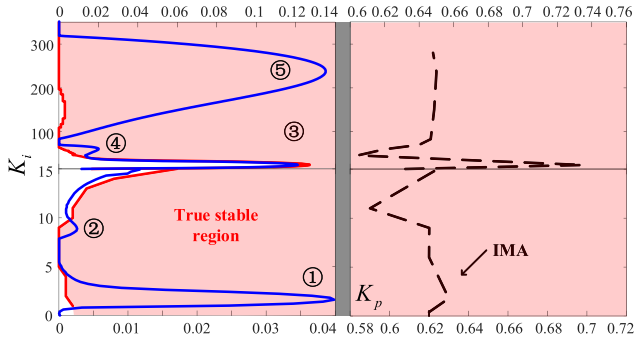

(c) Torsional dynamics of SG, dynamics of PMSG2, current control inner loops and reactive power control outer loop of GSC of PMSG1 are removed such that reduction of stable region around ①, ②, ④ and ⑤ disappears

Fig. 8. Computational results of stable regions in the parameter space of PLL1 when dynamics associated with the oscillation modes of ROPS subsystem are removed consecutively in three steps.

For the clear presentation, results computed by the PDA are not displayed in Fig. 8.

Following remarks can be made from the above test results.

1) Reduction of stable regions in the parameter space of PLL1 around points ①, ②, ③, ④ and ⑤ in Fig. 7 are due to the open-loop modal resonance between the PLL and ROPS subsystem. Around those points, dynamic interactions between PLL and ROPS subsystems are strong and degrade the SSO stability of example power system.
2) Negative resistance and negative net damping are highly related with the strong dynamic interactions caused by

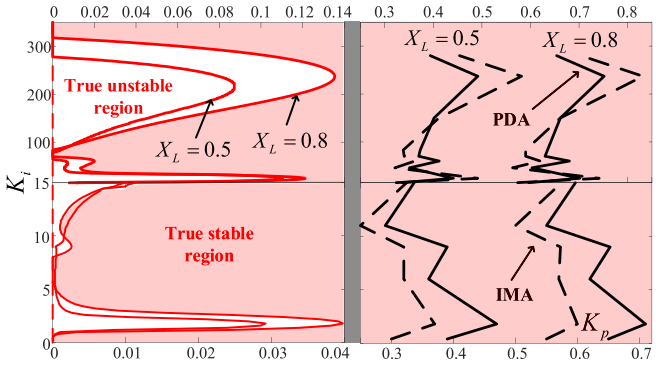

Fig. 9. Stable regions in the parameter space of PLL1 when condition of grid connection of PMSG1 varies.

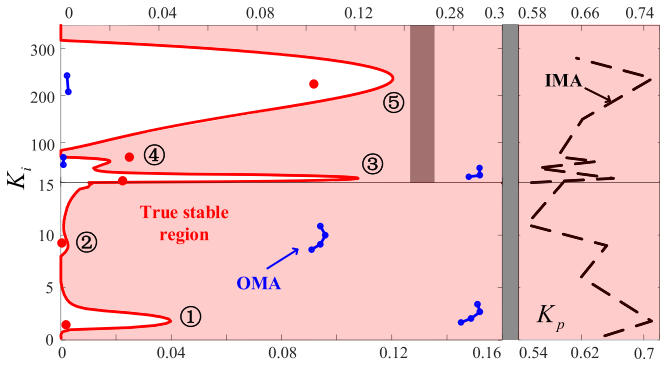

Fig. 10. Boundaries of stable regions computed by the OMA.

the open-loop modal resonance. With the elimination of open-loop modal resonance, dynamic interactions weaken and stable regions indicated by the IMA and PDA increase subsequently. This confirms the analysis made in Section II-C about the connection of the OMA with the IMA and PDA. Without making the comparison, this general feature of IMA and PDA may not be revealed.

3) Physical causes of SSO instability have been found being related with the torsional dynamics of SG, the PLL and converter control systems of grid-connected WTGs [2]–[16]. However, they were explained from the standpoints of negative resistance, negative net damping or modal resonance separately [9]–[16]. Fig. 8 shows that the physical components are responsible for the SSO problem as being found in [7], [8]. They are torsional dynamics of SG, the PLL and converter control systems of grid-connected WTGs. The IMA, the PDA and the OMA just provide the interpretation about the responsibility of same physical components from different perspectives. Fig. 8 clearly indicates that if the parameters of PLL1 are set improperly, modal resonance may happen and at the same time, resistance or the net damping of PLL1 becomes negative. Subsequently, the SSO instability occurs. Without the comparison between the OMA, the IMA and the PDA, this important insight may not be clearly demonstrated.

In addition to the dynamic interactions, the condition of grid connection of the WTG has been found to be an important factor to affect the impact of the WTG on system stability [7], [8]. In the example power system of Fig. 5, the reactance of transmission line connecting the wind-thermal bundled generation at the sending end to the AC grid is reduced from $X_L = 0.8$ p.u. to $X_L = 0.5$ p.u. Stable regions of the example power system in the parameter space of the PLL are computed. The computational results are displayed in Fig. 9 and compared with those before the reduction of the reactance of the transmission line. From Fig. 9, it can be seen that the true stable regions expand with the reduction of X_L. The trend of expansion is well captured by the IMA and PDA, as the boundaries of stable regions calculated by the IMA and PDA move towards the left on the parameter space of the PLL. The movement indicates that the example power system become more stable as far as the parameter setting of the PLL is concerned. Indeed, the condition of grid connection of the WTG (X_L) is a physical cause that the PMSG affects the stability of the example power system. The reason is that the dynamic interactions between PLL1 and the ROPS decrease when the grid connection is strengthened, resulting the increase of system stability.

C. Limitations of the IMA, the PDA and the OMA

Stability of interconnected system of Fig. 6 can be assessed by using the OMA, i.e., the SIC defined in (16), when the modal resonance happens. Hence, around five points indicated by the solid circles in Fig. 7, $(K_{pi}, K_{ii}), i = 1, 2, 3, 4, 5$, in the parameter space of PLL1, boundaries of stable regions are computed approximately by using the OMA. For the computation, when difference between the real and imaginary part of oscillation mode of PLL subsystem, λ_p, and that of oscillation modes of ROPS subsystem, $\lambda_{ri}, i = 1, 2, 3, 4, 5$, is less than 20% of real part of λ_p and 10% of imaginary part of λ_p, it is considered that modal resonance, $\lambda_p \approx \lambda_{ri}, i = 1, 2, 3, 4, 5$, happens. Then, stability of interconnected system of Fig. 6 is assessed by the SIC defined in (16). Consequently, boundaries of stable regions are obtained from the assessment and are displayed in Fig. 10 by solid circles connected by curves.

From Fig. 10, it can be seen that when the interconnected system of Fig. 6 is assessed being stable by the IMA, it is assessed being stable by the OMA. This confirms the connection between the IMA and OMA established in Section II-C. Assessment by the OMA is much closer to the true boundaries of stable region than that by the IMA. However, in the area of the parameter space of PLL1 where no modal resonance happens, the assessment by the OMA is not applicable. Hence, comparison displayed in Fig. 10 clearly shows the limitation of the OMA: For the case of SSO instability irrelevant with the dynamic interactions, the OMA cannot be used as effectively as the IMA and PDA.

In the parameter space of the PLL shown by Fig. 7, four points are selected and indicated by crosses in Fig. 7. They are point A $(K_p = 0.028, K_i = 1.8)$, B $(K_p = 0.40, K_i = 1.8)$, C $(K_p = 0.62, K_i = 1.8)$ and D $(K_p = 1.0, K_i = 1.8)$. From the boundary of true stable region in Fig. 7 (solid curve), it can be seen that at point A, the example power system is unstable and at other three points, the system is stable. At those four points, resistance of the PLL is computed. Computational

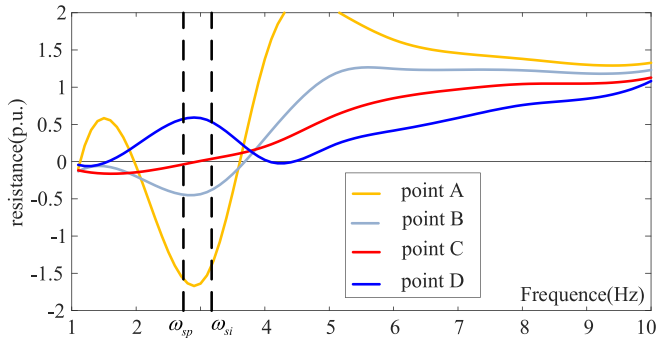

Fig. 11. Resistance vs frequency of the PLL at four points (A, B, C and D) in Fig. 7.

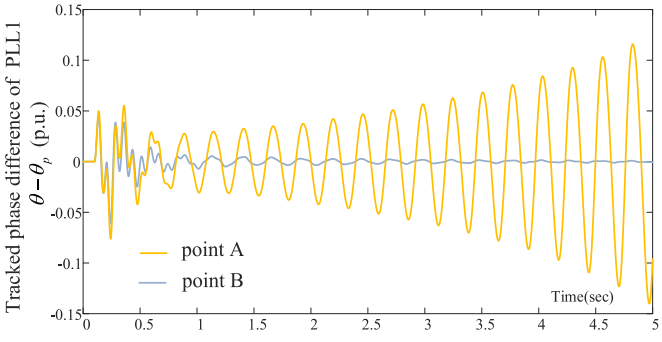

Fig. 12. Results of non-linear simulation.

results are presented in Fig. 11, where two vertical lines indicate the frequency, ω_{si} and ω_{sp}. ω_{si} is calculated according to (3) for the IMA to make the stability assessment. ω_{sp} is calculated by using (7) for the PDA to assess the system stability. Following observations can be made from Fig. 11.

1) At point C, resistance of the PLL at ω_{si} is positive but at ω_{sp} the net damping is negative. Thus, the PDA indicates that there is instability risk when $K_p = 0.62, K_i = 1.8$. However, the assessment from the IMA is that there is no problem of instability at all because the resistance is positive. The different stability assessment is caused by the difference between ω_{si} and ω_{sp}.
2) At point B, both the IMA and the PDA indicate that there is instability risk because the resistance or net damping of the PLL is about -0.47. However, the system in fact is stable. When only at point A, the system is unstable, where the resistance of the PLL is about -1.58, much smaller than the resistance at point B. Hence, the assessment made by the IMA and PDA is very conservative.
3) At point D where $K_p = 1.0, K_i = 1.8$, both the IMA and the PDA indicate that the power system is stable. However, at point B where $K_p = 0.4, K_i = 1.8$, the system is already stable. This implies that if the proportional gain of the PLL is set by using either the IMA or the PDA, the setting is over big.

Confirmation from non-linear simulation is presented in Fig. 11. At 0.1 second of simulation, active power output from PMSG1 increased by 10% for 0.1second. Fig. 12 shows two

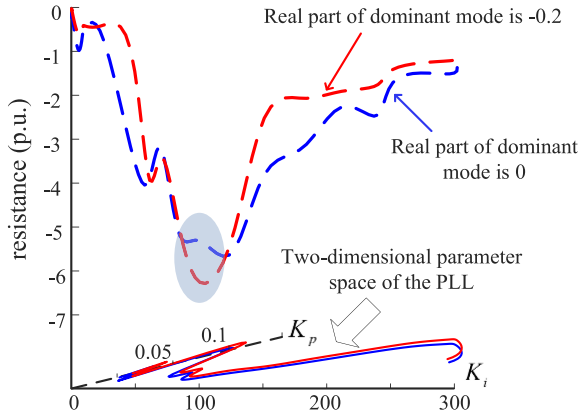

Fig. 13. Resistance of the PLL calculated by the IMA.

results of non-linear simulation: (1) Gain setting of the PLL is $K_p = 0.028, K_i = 1.8$ (point A in Fig. 7) when the power system is unstable; (2) Gain setting of the PLL is $K_p = 0.40, K_i = 1.8$ (point B in Fig. 7) when the power system is stable.

Results presented in Fig. 11 demonstrate the limitation of the IMA and PDA to detect the instability risk of the example power system. They may not only result in over setting of proportional gain of the PLL, but also provide wrong indication of system instability. The latter limitation can be demonstrated further by following study case.

First, gains of the PLL are set such that the most poorly damped oscillation mode of example power system is located on the imaginary axis of the complex plane. Setting values of the gains of PLL form a curve in the parameter space of the PLL. This curve in fact is a part of boundary of true stable region in Fig. 7 and displayed in dashed curve in the two-dimensional parameter space of the PLL in Fig. 13 (two-dimensional plane (K_p, K_i)). For each point on the dashed curve in Fig. 13, the resistance of the PLL at the resonance frequency ω_{si} is calculated by the IMA. Subsequently, the calculation maps the dashed curve in the two-dimensional parameter space of the PLL to form a curve (dashed curve) in the three-dimensional space, $(\text{resistance},\ K_p, K_i)$, as shown in Fig. 13. Hence, if in Fig. 13, resistance is negative, the IMA indicates that there may be instability risk of example power system.

Second, gains of the PLL are varied such that the real part of the most poorly damped oscillation mode of example power system is kept -0.2. Setting values of the gains of PLL form a curve in the parameter space of the PLL and is displayed in solid curve in the two-dimensional parameter space of the PLL in Fig. 13. Mapping of the red curve to the resistance calculated by the IMA forms a curve (solid curve) in the three-dimensional space as shown in Fig. 13. Following observations can be made from Fig. 13.

1) On each of two curves in the two-dimensional space of the PLL, stability of example power system is, in fact, unchanged as the real part of dominant oscillation mode is identical to be either 0 or -0.2. However, resistance calculated by the IMA varies. Hence, the variation of resistance actually means nothing as far as the system instability risk is concerned.

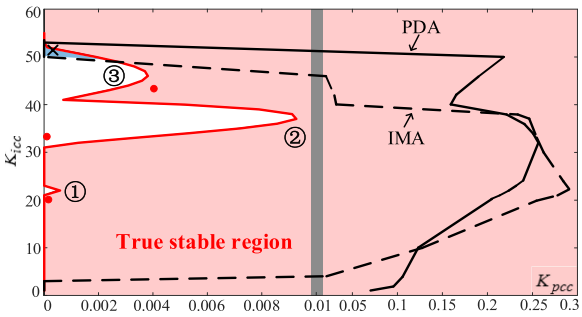

Fig. 14. Stable regions in the parameter space of CCIL1.

2) In the shadowed area, resistance indicated by the solid curve is smaller than that indicated by the dashed curve (more negative resistance). The indication is meaningless because in fact the example power system is more stable when the gains of the PLL are set such that the real part of dominant oscillation mode is -0.2.

Therefore, when either the IMA or PDA is used to examine the mechanism of power system SSOs caused by the grid-connected WTG, results of examination need to be interpreted carefully by considering the limitations of the IMA and PDA as demonstrated above.

TABLE II
SSO MODES OF ROPS SUBSYSTEM AND PARAMETERS OF CCIL1 TO CAUSE THE OPEN-LOOP MODAL RESONANCE

SSO modes of the ROPS subsystem	Dynamics associated with the SSO modes	Values of PI gains of CCIL1 to cause the modal proximity
$\lambda_{r1} = -0.09+j161$	The 3rd torsional SSO mode of SG	$K_{pcc1} = 0.000, K_{icc1} = 20$
$\lambda_{r2} = -0.10 + j204$	The 4th torsional SSO mode of SG	$K_{pcc2} = 0.000, K_{icc2} = 33$
$\lambda_{r3} = -2.90 + j236$	The CCIL of GSC of DFIG2	$K_{pcc3} = 0.004, K_{icc3} = 43$

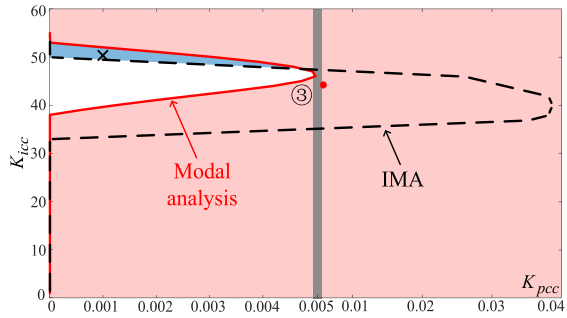

Fig. 15. Torsional dynamics of SG are removed such that reduction of stable region around ① and ② disappears.

IV. AN EXAMPLE POWER SYSTEM WITH GRID-CONNECTED DFIGS

A. Causes of Reduction of Stable Regions

Configuration of an example power system with grid-connected DFIGs is as same as that of previous example shown by Fig. 5. At the sending end, there are two grid-connected DFIGs instead of two PMSGs. Model and parameters of DFIG used in [20] are adopted. Other parameters of the example power system are given in Appendix. A TITO interconnected model of the example power system is derived. Configuration of the TITO interconnected model is shown by Fig. 1 where the WTG subsystem is comprised of DFIG1 and the ROPS subsystem consists of DFIG2, SG and network. Stable region of the example power system is computed by using the modal analysis in the parameter space of current control inner loop (CCIL) of rotor side converter (RSC) of DFIG1, referred to as CCIL1. Computational results are displayed as the shadowed area surrounded by the solid curve in Fig. 14, where K_{pcc} and K_{icc} are the proportional and integral gain of CCIL1 respectively.

In Fig. 14, dashed curve and dotted curve are the boundaries of stable regions computed by the IMA and PDA separately. It can be seen that when it is assessed by either the IMA or the PDA that the system is unstable (negative resistance or net damping), in fact the system may still be stable. Consequently, the conservative assessment made by the IMA and the PDA might lead to setting of over-big value of K_{pcc}. Particularly, in the area highlighted in grey, the system is assessed by the IMA being stable. However, the area is in the true unstable region such that the system is actually unstable. This error is caused by the simplification (*assumption 1*) from the TITO interconnected model to the SISO interconnected model based on which the IMA and PDA are applied, as discussed in Section II-A.

In Fig. 14, true stable region reduces around points ①, ② and ③ due to the dynamic interactions between DFIG1 and the ROPS, because the true stable region would be the right half of two-dimensional parameter space of CCIL1 if dynamics of ROPS are not considered. For confirmation, the first and second column in Table II present the computational results of SSO modes of ROPS subsystem, $\lambda_{ri}, i = 1, 2, 3$, and the dynamics associated with the SSO modes respectively. By setting the oscillation mode of DFIG1 associated with the CCIL1, λ_c, to be equal to the SSO modes of the ROPS, i.e., $\lambda_c = \lambda_{ri}, i = 1, 2, 3$, values of PI gains of CCIL1 are computed and computational results are listed in the third column of Table II. Those pairs of values, $(K_{pcck}, K_{icck}), k = 1, 2, 3$, are three points in the parameter space of CCIL1 which are indicated by solid circles in Fig. 14. Around the solid circles, open-loop modal proximity between DFIG1 and the ROPS happens. It can be seen that indeed the reduction of true stable region occurs around the points where open-loop modal resonance happens in the example power system.

Further confirmation is presented in Fig. 15 and Fig. 16. First, torsional dynamics of SG in the example power system are removed and then true stable region is computed. Computational results are displayed in Fig. 15. It can be seen that reduction of true stable region around points ① and ② in Fig. 14 disappears in Fig. 15 when the open-loop modal resonance between DFIG1 and torsional dynamics of SG does not happen. Second, integral gain of CCIL of DFIG2 is tuned from $K_{icc} = 165$ to $K_{icc} = 130$ such that λ_{r3} changes from$\lambda_{r3} = -2.90 + j236$ to $\lambda_{r3} = -2.53 + j209$. Subsequently, the point of open-loop

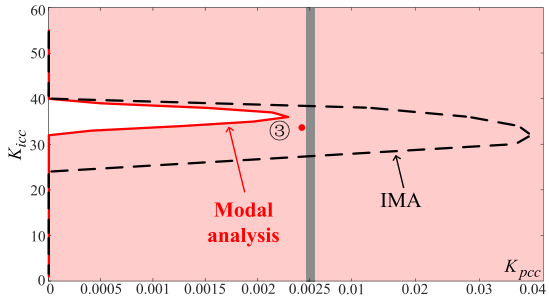

Fig. 16. Torsional dynamics of SG are removed and integral gain of CCIL of DFIG2 is tuned such that reduction of stable region around ① and ② disappeared and reduction area around ③ moves down.

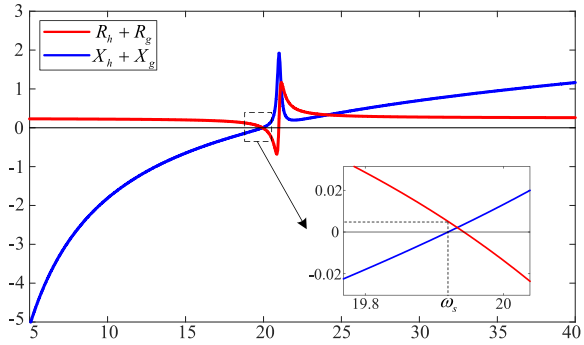

Fig. 17. Impedance-frequency computation at the point in the grey area of Fig. 14.

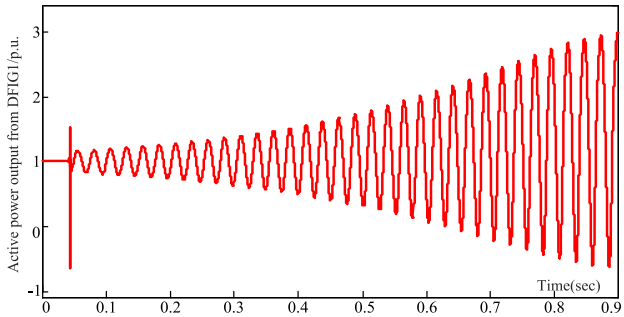

Fig. 18. Results of non-linear simulation.

modal resonance between DFIG1 and DFIG2 moves down in the parameter space of CCIL1 as indicated in Fig. 16. It can be seen that with the moving down of point of open-loop modal resonance, area of reduction of true stable region moves down. This confirms that the reduction of true stable region is caused by the open-loop modal resonance.

B. Limitation of the IMA

Computational results presented from Fig. 14 to Fig. 16 validate the connection between the IMA, the PDA and the OMA: The stable regions calculated by the IMA and PDA reduce as caused by the dynamic interactions between DFIG1 and the ROPS under the condition of open-loop modal resonance. The dynamic interactions are the cause that the IMA and PDA respectively give negative resistance and negative net damping respectively to indicate the danger of system SSO instability. However, indication by the IMA and PDA is very conservative. The indication may not be very useful in examining the SSO instability risk of the power system. This aspect has been well evaluated and demonstrated in the previous section. In this subsection, a further limitation of the IMA is demonstrated.

In the area highlighted in grey in Fig. 14, the example system is assessed to be stable by the IMA. However, the system, in fact, is unstable. This wrong assessment made by the IMA is caused by the simplification of the TITO interconnected model to the SISO interconnected model as being illustrated in Fig. 4. A further evaluation is conducted as follows.

A point marked by cross in the grey area in Fig. 14 is selected. At the point, gain values of CCIL1 are $K_{pcc} = 0.001, K_{icc} = 50$. When the gain values are taken by the CCIL1, the IMA is applied to assess system stability. Results of assessment are presented in Fig. 17. It can be seen that the resistance of the example power system defined by the IMA is 0.0052. However, this assessment made by the IMA about the system stability is wrong because the system is in fact unstable.

Confirmation from non-linear simulation is presented in Fig. 18 with $K_{pcc} = 0.001, K_{icc} = 50$. At 0.04 second of simulation, the voltage at the terminal of AC grid dropped by 10% and recovered in 0.001 second. It can be seen that the example power system is unstable and hence the assessment made by the IMA is incorrect.

V. Conclusion

This paper compares three main methods for studying the mechanism of the SSOs caused by the grid connection of WTGs. The comparison reveals the difference and connections between three methods, which helps to gain better understanding of the general mechanism of the SSOs caused by the grid-connected WTGs. Analysis and conclusions made by the comparison are evaluated and demonstrated by study cases, focusing on the impact of the PLL for a grid-connected PMSG and the current control inner loop of RSC of a grid-connected DFIG. Following important aspects of the SSOs caused by the grid-connected WTGs, as being examined by the IMA, the PDA and the OMA, are revealed and validated by the comparing study in the paper.

1) Stability assessment made by the IMA and PDA are highly related with the dynamic interactions between the grid-connected WTG and the ROPS. Under the condition of modal resonance, dynamic interactions are strong which may very possibly for the IMA or PDA to indicate negative resistance or net damping. This explains why the resistance or net damping may become negative from the standpoint of modal resonance.
2) Both the assessment made by the IMA and the PDA are based on the sufficient condition of system stability. They can reflect the trend of variation of system stability. However, they may provide incorrect indication of instability risk brought about by the grid-connected WTG. In fact, variation of resistance and net damping may be meaningless as far as the system SSO instability is concerned.

Hence, extra care needs to be taken to interpret the indication from the IMA and PDA. For the same reason, it is possible that the IMA and PDA may generate over-restricted results of control parameter setting in order to ensure the system stability.

3) In case that a TITO interconnected model is considered, the IMA and the PDA may give incorrect indication of system SSO stability due to the simplification of the TITO model to the SISO model.
4) The OMA is based on the approximation of sufficient and necessary condition of system stability. Hence, it can be used not only to ensure the system stability, but also to detect the system instability. However, the approximation may lead to wrong assessment by the OMA. In addition, the OMA is not applicable to the cases of non-modal resonance.
5) The connection between the OMA and IMA is established as follows: When the assessment of system stability made by the IMA is positive, the assessment made by the OMA is positive either. Hence, under the condition of modal resonance, the assessment made by the OMA is less conservative than that by the IMA and PDA as far as the system stability is concerned.
6) Assessment made by the IMA and PDA may be different. The difference is caused by the calculation of frequency, at which the resistance and the net damping is computed.

Possible directions of further study to improve the IMA, the PDA and the OMA can be summarized as follows.

1) It is important to detect the SSO instability risk which may be brought about by the grid connection of WTGs. Hence, development of new method of IMA based on the necessary condition of system stability is an essentially important work in near future.
2) The IMA and PDA are applicable by using the measurement data. This is their major advantage. Application of the OMA requires the modal information of open-loop subsystems. Hence, to develop algorithms to obtain such information by using the measurement data is an important work in near future in order to make the OMA applicable without the need to derive the parametric models.
3) For applying the IMA and PDA by using the measurement data, frequency response of WTG subsystem in Fig. 1 needs to be obtained by conducting field tests. This seems not a problem as the WTG being examined can be disconnected from the grid and then frequency response of the WTG is measured by injecting test signals with variable frequency at the terminal of the WTG. However, frequency response of the WTG obtained in this way, in fact, is not the frequency response of the WTG required for assessing its impact on the SSO stability of the power system, because the WTG is connected to the grid when it affects the system stability. Using the frequency response of disconnected WTG to represent that of grid-connected WTG assumes that the frequency response of the disconnected WTG remains unchanged when it is connected to the grid. This assumption does not generally stand. For example, when the active power output of the grid-connected WTG changes, its frequency response varies. Hence, frequency response of disconnected WTG (active power output is zero) usually cannot represent that of grid-connected WTG. Subsequently, stability assessment by using the frequency response of disconnected WTG may possibly be wrong.

Therefore, to apply the IMA or PDA, how to obtain the frequency response of WTG subsystem with the WTG being connected to the grid is a key problem to be solved. A technically feasible solution to the problem will make the IMA and PDA truly applicable in the field.

APPENDIX

See Tables III–VI.

TABLE III
LINE PARAMETERS OF EXAMPLE POWER SYSTEM WITH TWO PMSGS

Line	X_1	X_2	X_3	X_L
Reactance (p.u.)	0.01	0.01	0.05	0.8

TABLE IV
POWER OUTPUT OF SENDING-END PMSGS AND SG

Power output	PMSG1	PMSG2	SG
Active power(p.u.)	0.3	0.3	0.4
Reactive power(p.u.)	0.15	0.15	/

TABLE V
LINE PARAMETERS OF EXAMPLE POWER SYSTEM WITH TWO DFIGS

Line	X_1	X_2	X_3	X_L
Reactance (p.u.)	0.05	0.05	0.05	0.3

TABLE VI
POWER OUTPUT OF SENDING-END DFIGS AND SG

Power output	DFIG1	DFIG2	SG
Active power(p.u.)	1	1	1
Reactive power(p.u.)	0	0	/

REFERENCES

[1] V. Vittal and R. Ayyanar, *Grid Integration and Dynamic Impact of Wind Energy*. New York, NY, USA: Springer, 2013.
[2] T. Sadamoto, A. Chakrabortty, T. Ishizaki, and J. Imura, "Retrofit control of wind-integrated power systems," *IEEE Trans. Power Syst.*, vol. 33, no. 3, pp. 2804–2815, May 2018.
[3] E. Vittal, M. O'Malley, and A. Keane, "Rotor angle stability with high penetrations of wind generation," *IEEE Trans. Power Syst.*, vol. 27, no. 1, pp. 353–362, Feb. 2012.
[4] E. Vittal and A. Keane, "Identification of critical wind farm locations for improved stability and system planning," *IEEE Trans. Power Syst.*, vol. 28, no. 3, pp. 2950–2958, Aug. 2013.
[5] L. P. Kunjumuhammed, B. C. Pal, C. Oates, and K. J. Dyke, "Electrical oscillations in wind farm systems: Analysis and insight based on detailed modeling," *IEEE Trans. Sustain. Energy*, vol. 7, no. 1, pp. 51–62, Jan. 2016.
[6] B. C. Pal and F. Me, "Modelling adequacy of the doubly fed induction generator for small-signal stability studies in power systems," *IET Renewable Power Gener.*, vol. 2, no. 3, pp. 181–190, Sep. 2008.
[7] S. Ma, H. Geng, L. Liu, G. Yang, and B. C. Pal, "Grid-synchronization stability improvement of large scale wind farm during severe grid fault," *IEEE Trans. Power Syst.*, vol. 33, no. 1, pp. 216–226, Jan. 2018.

[8] L. P. Kunjumuhammed, B. C. Pal, R. Gupta, and K. J. Dyke, "Stability analysis of a PMSG-based large offshore wind farm connected to a VSC-HVDC," *IEEE Trans. Energy Convers.*, vol. 32, no. 3, pp. 1166–1176, Sep. 2017.
[9] L. Fan and Z. Miao, "Nyquist-stability-criterion-based SSR explanation for type-3 wind generators," *IEEE Trans. Energy Convers.*, vol. 27, no. 3, pp. 807–809, Sep. 2012.
[10] Z. Miao, "Impedance-model-based SSR analysis for type 3 wind generator and series-compensated network," *IEEE Trans. Energy Convers.*, vol. 27, no. 4, pp. 984–991, Dec. 2012.
[11] L. Harnefors, M. Bongiorno, and S. Lundberg, "Input-admittance calculation and shaping for controlled voltage-source converters," *IEEE Trans. Ind. Electron.*, vol. 54, no. 6, pp. 3323–3334, Dec. 2007.
[12] J. Lyu, X. Cai, and M. Molinas, "Frequency domain stability analysis of MMC-based HVdc for wind farm integration," *IEEE J. Emerg. Sel. Topics Power Electron.*, vol. 4, no. 1, pp. 141–151, Mar. 2016.
[13] H. Liu, X. Xie, C. Zhang, Y. Li, H. Liu, and Y. Hu, "Quantitative SSR analysis of series-compensated DFIG-based wind farms using aggregated RLC circuit model," *IEEE Trans. Power Syst.*, vol. 32, no. 1, pp. 474–483, Jan. 2017.
[14] L. Harnefors, "Proof and application of the positive-net-damping stability criterion," *IEEE Trans. Power Syst.*, vol. 26, no. 1, pp. 481–48, Feb. 2011.
[15] M. Cheah-Mane, L. Sainz, J. Liang, N. Jenkins, and C. E. Ugalde-Loo, "Criterion for the electrical resonance stability of offshore wind power plants connected through HVDC links," *IEEE Trans. Power Syst.*, vol. 32, no. 6, pp. 4579–4589, Nov. 2017.
[16] W. Du, X. Chen, and H. F. Wang, "A method of open-loop modal analysis to examine the SSOs in a multi-machine power system with multiple variable speed wind generators," *IEEE Trans. Power Syst.*, vol. 33, no. 4, pp. 4297–4307, Jul. 2018.
[17] L. Harnefors, "Modeling of three-phase dynamic systems using complex transfer functions and transfer matrices," *IEEE Trans. Ind. Electron.*, vol. 54, no. 4, pp. 2239–2248, Aug. 2007.
[18] IEEE Subsynchronous Resonance Task Force, "First benchmark model for computer simulation of subsynchronous resonance," *IEEE Trans. Power App. Syst.*, vol. PAS-96, no. 5, pp. 1565–1572, Sep. 1977.
[19] W. Du, X. Chen, and H. F. Wang, "PLL-induced modal resonance of grid-connected PMSGs with the power system electromechanical oscillation modes," *IEEE Trans. Sustain. Energy*, vol. 8, no. 4, pp. 1581–1591, Oct. 2017.
[20] L. Fan, R. Kavasseri, Z. L. Miao, and C. Zhu, "Modeling of DFIG-based wind farms for SSR analysis," *IEEE Trans. Power Del.*, vol. 25, no. 4, pp. 2073–2082, Oct. 2010.

Wenjuan Du (M'14) received the Ph.D. degree from the University of Bath, Bath, U.K., in 2009. She is currently with the School of Electrical Engineering, Sichuan University, Chengdu, China. Her main research interests focus on power system stability analysis and control, including energy storage systems, FACTS, EV, and renewable power generations.

Bixing Ren received the Ph.D. degree from the School of Electrical and Electronic Engineering, North China Electric Power University, Beijing, China, in 2019. He is currently an Electrical Engineer with the State Grid Jiangsu Electric Power Company Ltd., Research Institute, Nanjing, China. His main research interests focus on power system stability analysis and control, including FACTS and renewable power generations.

Haifeng Wang (M'96–SM'02) is currently a Full Professor with the School of Electrical and Electronic Engineering, North China Electric Power University, Beijing, China. He is also with the State Key Laboratory of Alternate Electric Power Systems with New Energy Resources, North China Electric Power University. He had worked in the U.K. for years and was the Chair in electrical engineering and a Full Professor with Queen's University Belfast, Belfast, U.K., before he moved to Beijing. His main research interest focuses on power system stability analysis and control.

Yang Wang is currently working toward the Ph.D. degree with the School of Electrical and Electronic Engineering, North China Electric Power University, Beijing, China. He is currently with the State Key Laboratory of Alternate Electric Power Systems with New Energy Resources, North China Electric Power University, Beijing, China. His main research interests focus on power system stability analysis and control, including renewable power generations.